The Dynamic Fracture Properties of Rocks under Confining Pressure

Kazuhiko SATO* Minoru KAWAKITA** Shigenori KINOSHITA**

(Received June 30, 1981)

Abstract

The impulsive loading tests under confining pressure were performed to investigate the dynamic fracture properties of rocks in a triaxial stress state. The apparatus used in this study consists of the split Hopkinson bar, a pressure vessel and a hydraulic actuator. Six kinds of sedimentary rocks were selected for the test. The experiments were made at the strain rate of the order 10^2 sec^{-1} and under a confining pressure varying from 0.1 to 35 MPa.

The stress-strain curves and fracture strength obtained in the tests were compared with those of the conventional triaxial tests. The fracture criterion of each rock deduced from both static and dynamic tests could be expressed by the linear equation $\sigma_1 = C_0 + q\sigma_3$, where σ_1 and σ_3 are fracture strength and confining pressure, C_0 is the uniaxial compression strength which increases with increasing strain rate and q is the coefficient of confining pressure which is not dependent on the strain rate.

These experimental results were discussed on the basis of linear fracture mechanics, assuming that the crack growth obeys in-plane shear mode.

It was concluded that the dynamic fracture properties of rocks were predominantly affected by crack density as well as a power appearing in the equation of slow crack growth $V = \alpha K_{II}^{B}$, where V and K_{II} denote the crack growth velocity and the stress intensity factor of in-plane shear mode, B and α are constants.

1. Introduction

There were many investigations on the dynamic fracture of rocks, aiming at the development of practical techniques such as rock-blasting, drilling, crushing and comminution. However there were not from a basic point of view many studies which treated the dynamic fracture properties of rock fundamentally. In the present study, attention was paid to elucidate the dynamic behavior of rock when it was sujected to the impulsive load, especially the effect of strain rate on the fracture strength.

For the purpose of creating a high strain rate in the rock specimen various loading methods were employed. A hydraulic or screw-driven testing machine is a

* Department of Mineral Development Engineering, Muroran Institute of Technology, Muroran 050, Japan

** Department of Mineral Resorces Development Engineering

conventional means for a low range of strain rate. For a higher range of strain rate, for example, the split Hopkinson bar tests[1)-4)], the method of applying an impulsive pressure to rock by electric detonator[5)] and the flying-plate test[6)] in which a rock specimen of flat plate is impacted by a metal plate have been used. Through the studies[7),8)] the effect of high strain rate on the fracture under uniaxial stress state seems to be fairly well understood. That in poly-axial stress state, however, was not yet clear although the experimental technique for the high velocity compression test under the confining pressure has been developed[3),4)].

From this point of view, the triaxial compression tests were performed by using the SHB (short for split Hopkinson bar) method as well as the convensional hydraulic testing machine. The experimental procedures and results will be described and the effects of strain rate and confining pressure on the strength of rock will be discussed on the basis of a crack propagating model.

2. Experimental procedures

A schematic view of the testing apparatus is shown in Fig.1. It consists of two elastic bars (indicated as input bar and output bar in the diagram), the pressure vessel for applying confining pressure to the specimen, the hydraulic actuator for adjusting the axial pressure to keep the specimen in contact with elastic bars and the compressed gas chamber for driving the impacting bar to hit the input bar. The elastic bars are made of special steel whose yield stress is approximately 0.5 GPa and both of them are 30 mm in diameter with a length of 800 mm and 500 mm respectively. The input bar has a cylindrical collar near the impact end to sustain the static pre-axial load applied by the actuator. The dynamic axial stress is generated by mechanical collision between the input bar and impacting bar which is

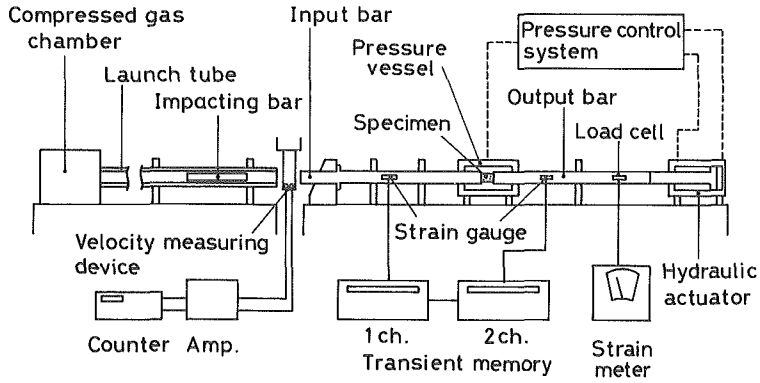

Fig. 1 Schematic view of the experimental arrangement and instrumentation.

launched through a 2 m long tube with a compressed nitrogen gas gun.

Maximum impact velocity is of the order 30 m/sec, limited by yield strength of the elastic bar. The impacting bar is made of the same material as the elastic bars

and its length is taken as 266 mm so that the duration of the stress wave in the input bar may be 100 μsec. The stress waves propagating in the bars are detected by means of the semi-conductor strain gauges mounted on both input bar and output bar, then memorized into the transient memories for writing down on X-Y recorder afterward.

In the tests the specimen was initially set under a hydrostatic pressure, then subjected to a dynamic axial stress whose intensity is sufficient to overcome the fracture strength. The confining presssure was varied from 0.1 to 35 MPa while the strain rate was of the order 10^2 sec^{-1}.

In addition to the SHB tests, conventional static triaxial tests were carried out under confining pressure, ranging from 0.1 to 100 MPa, and at a strain rate of 10^{-5} sec^{-1} in order to compare the dynamic fracture properties with the static ones.

3. Specimens

Some physico-mechanical properties of each rock specimen used in this study are shown in Table 1. All the test specimens were prepared as right circular cylinders 25.0 mm both in diameter and length. They were prepared as drilled cores and were finished with a surface grinder and lapping machine to have a flatness and

Table 1. Rock type and some physico-mechanical properties.

ROCK TYPE	True specific gravity γ	Porosity ϕ (%)	P wave velocity Vp (Km/sec)	Uniaxial compressive strength C_{os} (MPa)
HORONAI sandstone	2.66	12.8	2.50	75
SUNAGAWA sandstone	2.64	3.8	3.11	99
HOROKABETSU shale	2.64	10.6	3.16	73
AKIYOSHI limestone (coarse grained)	2.72	0.9	5.37	75
AKIYOSHI limestone (fine grained)	2.71	0.5	6.00	101
OGINO tuff	2.60	25.8	2.92	64

parallelism within 0.01 mm.

4. Experimental results

4. 1 Stress-strain curves

An example of the stress wave records obtained in the experiment is given in

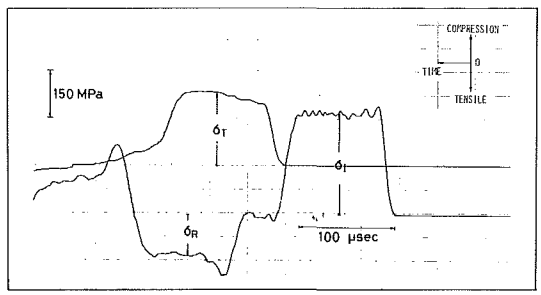

Fig. 2 Example of the stress wave records.

Fig. 2. The upper trace is the stress wave of the output bar and the lower trace is that of the input bar. The right rectangular pulse on the lower trace is the incident wave produced by impact, while the left one is part of the incident wave reflected from the specimen-input bar interface. The pulse on the upper trace is the transmitted wave to the output bar through the specimen.

The stress-strain relation for a specimen can be obtained by analyzing these stress waves. Provided that the stresses at both ends of the specimen are not greatly different, the stress σ, strain rate $\dot{\varepsilon}$ and strain ε can be expressed respectively as follows,

$$\sigma = \frac{A_0}{A} \frac{\sigma_I + \sigma_R + \sigma_T}{2} \tag{1}$$

$$\dot{\varepsilon} = \frac{1}{\rho c a}(\sigma_I - \sigma_R - \sigma_T) \tag{2}$$

$$\varepsilon = \frac{1}{\rho c a}\int_0^t (\sigma_I - \sigma_R - \sigma_T)dt \tag{3}$$

where, σ_I, σ_R, σ_T ; stress amplitude of incident, reflected and transmitted waves respectively,

A_0, A ; cross-sectional areas of elastic bar and specimen,

ρ ; density of elastic bar,

c ; wave velocity of elastic bar,

a ; length of specimen.

t ; loading time.

Accordingly, we can obtain the stress-strain curve by eliminating time t from Eqs.(1) and (3).

Some examples of the stress-strain curves derived for HORONAI sandstone are

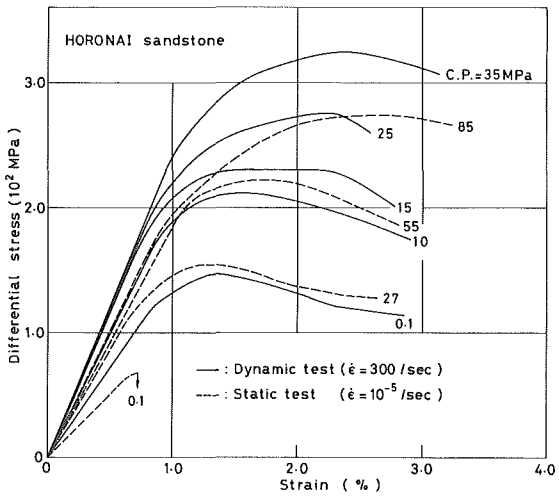

Fig. 3 Typical stress-strain curves of HORONAI sandstone together with the static stress -strain curves.

shown in Fig. 3, together with the static stress-strain curves.

The average strain rate at the dynamic tests is 300 sec^{-1} and that at the static tests is $10^{-5}sec^{-1}$.

It may be seen from the curves that the stress-strain relationships in the dynamic tests under 0.1 and 10 MPa confining pressure coincides approximately with those of 27 and 55 MPa confining pressure in the static tests respectively. The brittle-ductile transition pressure, at which the dominant deformation changes from brittle to ductile, seems to be about 50 to 80 MPa in the static test. On the other hand, in the dynamic case, the transition confining pressure is fairly lower ranging from 10 to 35 MPa. These results show that the deformation behavior of rock in triaxial stress state becomes ductile at lower confining pressures in the dynamic condition than in the static condition. This implies that rocks are inclined to be more ductile as the strain rate increases.

4. 2 The dynamic fracture strength under confining pressure

The fracture strength-confining pressure relations for six kinds of rocks are shown in Fig. 4(a) to (f), together with those of static tests, where the fracture strength is defined as the stress when the slope of stress-strain curve equals zero.

It is noteworthy that the dynamic strength curve relative to confining pressure is almost in parallel with to the static one for every rock type. Therefore, the fracture criterion can be expressed for both dynamic and static test by the Coulmb -Mohr hypothesis, namely,

$$\sigma_1 = C_0 + q\sigma_3 \qquad (4)$$

where σ_1 and σ_3 are the fracture strength and confining pressure, C_0 is the uniaxial compressive strength which increases with the strain rate and q is a coefficient

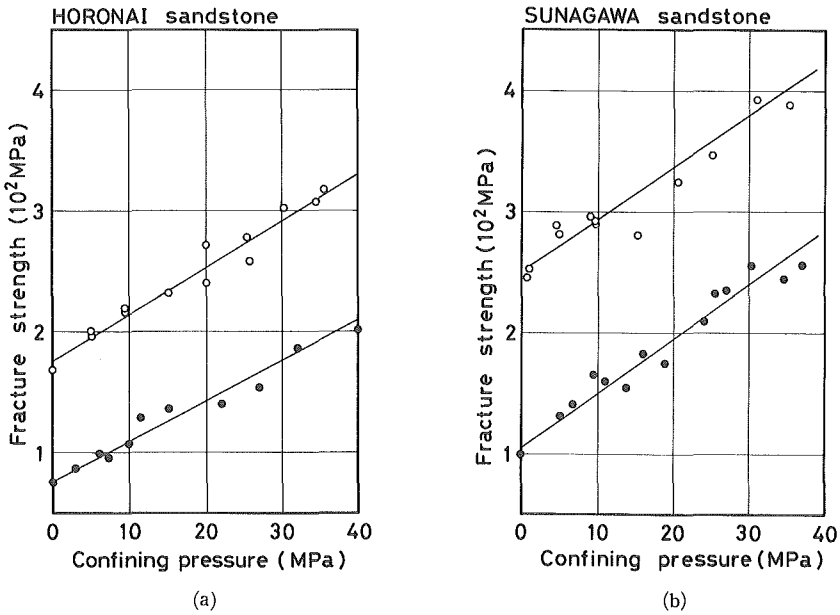

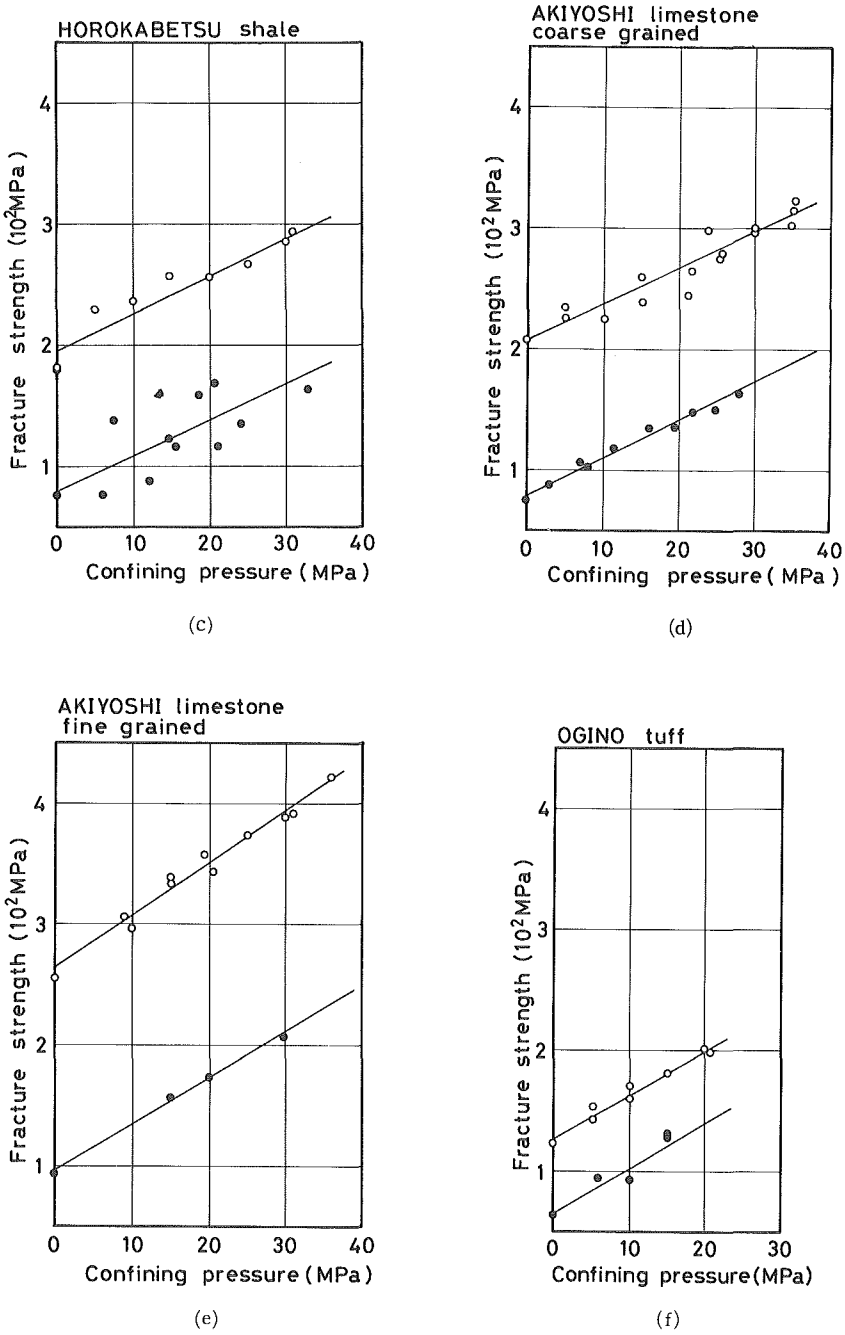

Fig. 4 Comparison between the dynamic and static fracture strength under confining pressure, ○; dynamic test ($\dot{\varepsilon}=300$/sec), ●; static test ($\dot{\varepsilon}=10^{-5}$/sec).

which is hardly influenced by the strain rate. The fracture criteria for each of six

Table 2. Fracture criterion of each rock deduced from both the static and dynamic tests; $\sigma_1 = C_0 + q\sigma_3$, C_{0s} and C_{0d} are the static and dynamic strength in uniaxial stress state, q_s and q_d are the coefficients of confining pressure at the static and dynamic tests.

ROCK TYPE	Cod (MPa)	Cos (MPa)	Cod/Cos	qd	qs	qd/qs
HORONAI sandstone	175	75	2.33	3.91	3.39	1.15
SUNAGAWA sandstone	250	105	2.38	4.39	4.55	0.96
HOROKABETSU shale	195	76	2.57	3.08	2.95	1.04
AKIYOSHI limestone (coarse grained)	208	79	2.63	3.97	3.19	1.24
AKIYOSHI limestone (fine graind)	265	96	2.76	4.39	3.82	1.15
OGINO tuff	125	64	1.95	3.68	3.79	0.97

kinds of rocks are summarized in Table 2.

5. Discussion

The dynamic fracture properties of rocks described in the preceding section will be considered on the basis of a proposed crack model. In fracture mechanics, it is described that three modes of deformation, namely, opening, in-plane shear, and anti-plane shear mode, may be possible near the crack tip when the material containing a crack is subjected to a stress state. Among them the shear deformation across the crack surfaces must be of a dominant mode in compression stress state since the cleavage mode of crack deformation would be arrested by the compressive normal stress near the crack tip.

On the observation mentioned above it is assumed that,

1) A large number of randomly oriented closed cracks are contained in an elastic body. The compliance of the body at the stationary state is greater than that of the solid part and increased with the growth of the cracks.

2) The crack growth is dominated by in-plane shear mode and the crack propagating velocity is postulated to follow the modified equation for the case of slow crack growth of the opening mode[9], namely,

$$V = \alpha K_{II}^{B} \qquad (5)$$

in which V is the velocity of crack growth, K_{II} denotes the stress intensity factor of in-plane shear mode, α and B are constants.

5. 1 The stress-strain relationship of the crack medium

Consider an elastic rectangular parallelepiped of a length h, width b and thickness u, containing a large number of randomly oriented closed cracks of 2a in average length and width per unit volume, and which is under a triaxial stress state. In this case the whole of body can be regarded as an isotropic one since the cracks of the same shape are oriented in such a random state.

Now let the effective Young's modulus and Poisson's ratio be E_{eff} and ν_{eff} respe-

ctively, the principal strain ε_1 in the direction of the maximum principal stress σ_1 can be expressed as follows,

$$\varepsilon_1=\frac{1}{E_{eff}}\{\sigma_1-\nu_{eff}(\sigma_2+\sigma_3)\} \tag{6}$$

where σ_2 and σ_3 are the intermediate and the minimum principal stresses. As the effective and intrinsic bulk moduli of the body containing closed cracks are equals[10], then,

$$\frac{1-2\nu_{eff}}{E_{eff}}=\frac{1}{3K}=\frac{1-2\nu}{E} \tag{7}$$

where K, E and ν are the intrinsic bulk modulus, Young's modulus and poisson's ratio of a solid body. Using Eq.(7), the principal strain ε_1 can be rewritten for triaxial stress state $\sigma_1 \geqq \sigma_2=\sigma_3$,

$$\varepsilon_1=\frac{\sigma_1}{E_{eff}}-\left(\frac{1}{E_{eff}}-\frac{1-2\nu}{E}\right)\sigma_3. \tag{8}$$

According to Walsh[11], the effective Young's modulus E_{eff} can be found by averaging all cracks for which sliding is possible.

This yields, for plane strain,

$$\frac{1}{E_{eff}}=\frac{1}{E}\left\{1+\frac{4(1-\nu^2)\pi a^3LN}{15}\left[\frac{2\mu^4+3\mu^2+2\mu}{(1+\mu^2)^{3/2}}-2\mu\right]\right\} \tag{9}$$

where L=1/bhu, N is the total number of cracks and μ is the coefficient of internal friction.

Substituting Eq.(9) into Eq.(8), we get

$$\varepsilon_1=\frac{\sigma_1}{E}\left(1+\frac{4\pi na^3LN}{15}\right)-\frac{\sigma_3}{E}\left(2\nu+\frac{4\pi na^3LN}{15}\right) \tag{10}$$

where $n=\left[\frac{2\mu^4+3\mu^2+2\mu}{(1+\mu^2)^{3/2}}-2\mu\right](1-\nu^2)$.

Eq.(10) represents the stress-strain relationship of the crack medium containing crack length and number of cracks as parameters.

For the sake of the numerical computation, we deform Eq.(10) to the expression in terms of dimensionless variables. From Eq.(10), the strain ε_0 at which the fracture is initiated under uniaxial compression can be written as,

$$\varepsilon_0=\frac{C_{0s}}{E}\left(1+\frac{4\pi na_0^3LN}{15}\right) \tag{11}$$

where C_{0s} is the uniaxial compressive strength in static condition (refer to Table 2) and a_0 is the crack semilength just as the stress attains C_{0s}. Then dividing Eq.(10) by Eq.(11), we can obtain the dimensionless form of Eq.(10), namely,

$$W=\frac{m+Ny^3}{m+N}z-\frac{p+Ny^3}{m+N}k \tag{12}$$

where $w=\frac{\varepsilon_1}{\varepsilon_0}$, $y=\frac{a}{a_0}$, $z=\frac{\sigma_1}{C_{0s}}$, $k=\frac{\sigma_3}{C_{0s}}$, $m=\frac{15}{4\pi na_0^3L}$, $p=\frac{15}{2\pi na_0^3L}$.

Differentiating Eq.(12) with respect to time t and making adjustments, we get the differential equation containing a term of strain rate R.

$$\frac{dz}{dx}=\frac{m+N}{m+Ny^3}R-\frac{3Ny^2}{m+Ny^3}(z-k)\frac{dy}{dx} \tag{13}$$

where $R=dw/dx$, $x=t/t_0$, t_0 ; time at which σ_1 equals C_{0S}.

5. 2 Crack growth in triaxial stress state

As previously mentioned, it is assumed that the deformation at the crack tip is dominated by in-plane shear mode.

At this situation the stress intensity factor K_{II} can be expressed as

$$K_{II}=\sqrt{\pi a}\tau_{eff} \tag{14}$$

where τ_{eff} represents the effective shear stress and a is the crack semilength.

Using the normal and shear stresses across the crack surfaces, denoted by σ_n and τ respectively, τ_{eff} in Eq.(14) is given by

$$\begin{aligned}\tau_{eff}&=|\tau|-\mu\sigma_n\\&=\frac{1}{2}(\sigma_1-\sigma_3)\ (\sin2\beta-\mathrm{con}2\beta)-\frac{1}{2}\mu(\sigma_1+\sigma_3)\end{aligned} \tag{15}$$

in the stress state of $\sigma_1\geqq\sigma_2=\sigma_3$, where β is the angle by which the normal to the plane of crack makes with the direction of σ_1. Relative motion between the surfaces of closed crack is possible only when $|\tau|>\mu\sigma_n$.

Then, similar to Eq.(9), the mean value of effective shear stress τ_{eff} in the body containing a large number of randomly oriented cracks can be obtained by averaging all cracks for $|\tau|>\mu\sigma_n$, that is, $\phi<\beta<\pi/2$,

$$\begin{aligned}\bar{\tau}_{eff}&=\int_0^{2\pi}\int_\phi^{\pi/2}\tau_{eff}\sin\beta\ d\beta\ d\theta\ /\int_0^{2\pi}\int_\phi^{\pi/2}\sin\beta\ d\beta\ d\theta\\&=\frac{1}{3}\frac{1-\sin\phi}{\cos\phi}\sigma_1-\frac{1}{3}\frac{1+2\sin\phi}{\cos\phi}\sigma_3\end{aligned}$$

or

$$\bar{\tau}_{eff}=\frac{1}{3}(\sqrt{1+\mu^2}-\mu)\sigma_1-\frac{1}{3}(\sqrt{1+\mu^2}+2\mu)\sigma_3 \tag{16}$$

where ϕ is the angle of internal friction defined by $\mu=\tan\phi$ and the direction of normal to the crack surface is specified by its longitude θ and zenith β of spherical coordinates.

Using $\bar{\tau}_{eff}$ instead of τ_{eff} in Eq.(14) and substituting that into Eq.(5), we can get the equation of motion, namely,

$$\begin{aligned}V&=\alpha(\sqrt{\pi a}\ \bar{\tau}_{eff})^B\\&=\alpha\pi^{B/2}a^{B/2}g_1^B\left(\sigma_1-\frac{g_2}{g_1}\sigma_3\right)^B\end{aligned} \tag{17}$$

where $g_1=(\sqrt{1+\mu^2}-\mu)/3$, $g_2=(\sqrt{1+\mu^2}+2\mu)/3$.

The velocity of crack growth V_0 when σ_1 attains C_{0S} can be written as

$$V_0=\alpha\pi^{B/2}\ a_0^{B/2}\ g_1^B\ C_{0S}^B \tag{18}$$

From Eqs.(17) and (18), the non-dimensional form of Eq.(17) will be given as follows,

$$\frac{dy}{dx}=y^{B/2}\ (z-f\ k)^B \tag{19}$$

where $f=g_2\ /\ g_1$.

Therefore the constitutive equations of the crack medium are given by the simultaneous differential equations of Eqs.(13) and (19).

5. 3 The results of numerical computations

In this section the effects of strain rate R and confining pressure k on the fracture strength z are investigated by solving the simultaneous differential equations

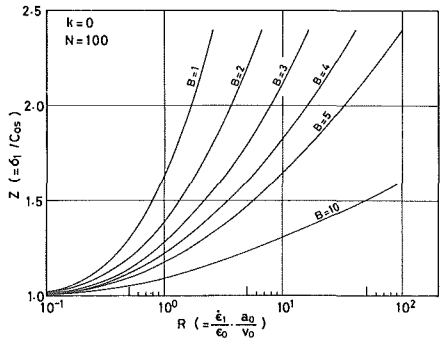

Fig. 5 Fracture strength z–strain rate R relations, varying B value as a parameter.

numerically. The Runge–Kutta–Gill method is used for computation.

Fig. 5 shows the fracture strength z vs. strain rate R for varying the value of power B in Eq.(19) under uniaxial stress state (k=0).

It is seen that the fracture strength increases with increasing strain rate while the strength rises more steeply with decreasing B value.

The z–R relation for the case of varying the number of cracks N is shown in Fig. 6. It can be observed from this figure that the shapes of curves are almost the

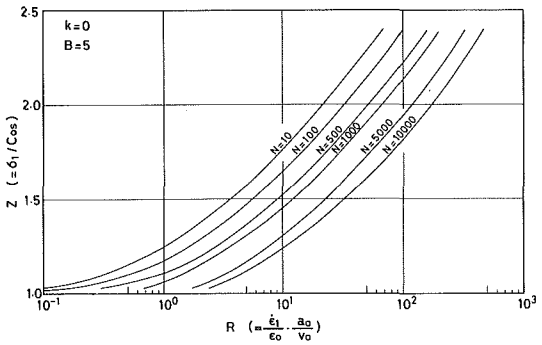

Fig. 6 Fracture strength z–strain rate R relations, varying N value as a parameter.

same in spite of the increase of N and that the curves are only shifted along the abscissa. For the same strain rate, the strength increases conspicuously as the number of cracks N decreases.

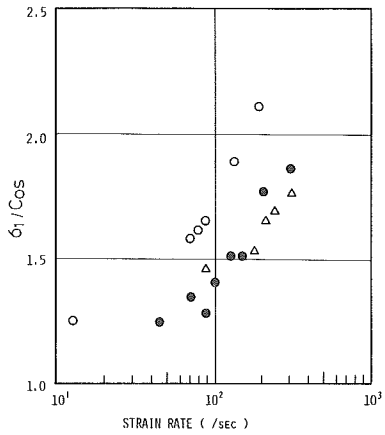

Fig. 7 Typical results of the SHB tests in uniaxial stress state, △ ; SUNAGAWA sandstone, ● ; AKIYOSHI coarse grained limestone, ○ ; AKIYOSHI fine grained limestone.

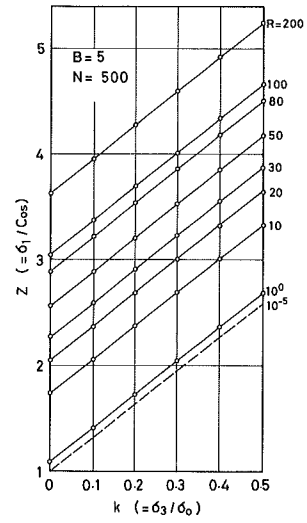

Fig. 8 Fracture strength z–confining pressure k relations, varying R value as a parameter: the dotted line is approximate one of the static experimental data, while the solid lines are the results of calculation.

Fig. 7 shows the typical results of SHB tests performed in uniaxial stress state[8]. From the figure it is obvious that the fracture strength imcreases exponentially as the strain rate increases. It is found that the results of computations are in good agreement with the experimental results if the value B and N are taken as 5 and the order of 10^2 respectively.

Further, the computation of the z–k relation were made for AKIYOSHI coarse grained limestone, showing the results in Fig.8. In this figure the dotted line represents the static experimental datum which is approximated by the method of least squares.

It will be seen that fracture strength increases linearly with the increase of confining pressure for a constant strain rate and that the curves are moving upward in parallel to the static line with increase of strain rate. This calculation results also coincide with the experimental results in Fig. 4(d).

From those facts, it is suggested that the effects of strain rate and confining pressure on the strength of rocks may be well explained by the crack propagating model proposed in the previous section.

6. Conclusions

The conclusions obtained in this study are summarized as follows.

(1) The dynamic deformation behavior of rocks in triaxial stress state becomes more ductile at a lower confining pressure than in the static condition, that is, rocks

are inclined to be more ductile as the strain rate is higher.

(2) The dynamic fracture strength increases linearly with the increase of the confining pressure and is in parallel to the curve of static strength. Therefore, the fracture criterion for both the dynamic and static triaxial tests can be expressed by the Coulomb-Mohr hypothesis, $\sigma_1 = C_0 + q\ \sigma_3$, where σ_1 and σ_3 are the fracture srength and the confining pressure, C_0 is the uniaxial compressive strength which increases with the strain rate and q is the coefficient of confining pressure which is not influenced by strain rate.

(3) The simulation as to the effect of high strain rate ($\dot{\varepsilon} > 10$/sec) and confining pressure on the fracture strength was made by means of linear fracture mechanics, assuming that the crack growth obeys the in-plane shear mode. The computation results were in good agreement with the experimental data in triaxial stress state as well as in uniaxial stress state.

Acknowledgment

Computations described in this paper were performed by using HITAC com puter system at the Computing Center of Hokkaido University.

References

1) Green S. J. and Perkins R. D. Uniaxial compression tests at varying strain rates on three geological materials. Proc. Tenth Sympo. Rock Mech., Univ. of Texas at Austin, 34–54, 1968.

2) Hakalehto K. O. Brittle fracture of rocks under impulsive load. Int. J. Fracture Mech. 6, 249–256, 1970.

3) Christensen R. J., Swanson S. R. and Brown W. S. Split Hopkinson bar tests on rocks under confining pressure. Experimental Mech. 12, 508–513, 1973.

4) Lindholm V. S., Yeakly L. M. and Nagy A. The dynamic strength and fracture properties of Dresser basalts. Int. J. Rock Mech. Sci. 11, 181–191, 1974.

5) Ito I. and Therada M. Compressidility of rock under impulsive high pressure. Materials, 13, 134, 885–890, 1964. (with English Abstract)

6) Shocky D. A., Curran D. R., Seaman L., RosebergJ. T. and Peterson C. F. Fragmentation of rock under dynamic loads. Int. J. Rock Mech. Min. Sci. 11, 303–317, 1974.

7) Kumar A. The effect of stress rate and temperature on the strength of basalt and granite. Geophysics. 33, 501–510, 1968.

8) Kinoshita S., Sato K., Kawakita M. On the mechanical behavior of rocks under impulsive loading. Bull. Faculty Eng. Hokkaido Univ. 83, 51–61, 1977. (with English Abstract).

9) Henry J. P., Paquet J. and Tancrez J. P. Experimental study of crack propagation in the calcite rocks. Int. J. Rock Mech. Sci, 14, 85–91, 1977.

10) Jeager J. C. and Cook N. G. W. Fundamentals of Rock Mechanics 2nd Ed., Chapman and Hall, p331, 1976.

11) Walsh J. B. The effect of cracks on the uniaxial elastic compression of rock. J. Geophs. Res. 70 (2), 392–401, 1965.